Observations of Small-Scale Turbulence and Energy Dissipation Rates in the Cloudy Boundary Layer

HOLGER SIEBERT, KATRIN LEHMANN, AND MANFRED WENDISCH

Leibniz-Institute for Tropospheric Research, Leipzig, Germany

(Manuscript received 6 December 2004, in final form 29 August 2005)

ABSTRACT

Tethered balloon–borne measurements with a resolution in the order of 10 cm in a cloudy boundary layer are presented. Two examples sampled under different conditions concerning the clouds' stage of life are discussed. The hypothesis tested here is that basic ideas of classical turbulence theory in boundary layer clouds are valid even to the decimeter scale. Power spectral densities $S(f)$ of air temperature, liquid water content, and wind velocity components show an inertial subrange behavior down to ≈20 cm. The mean energy dissipation rates $\bar{\varepsilon}$ are $\sim 10^{-3}$ m^2 s^{-3} for both datasets. Estimated Taylor Reynolds numbers (Re_λ) are $\sim 10^4$, which indicates the turbulence is fully developed. The ratios between longitudinal and transversal $S(f)$ converge to a value close to 4/3, which is predicted by classical turbulence theory for local isotropic conditions. Probability density functions (PDFs) of wind velocity increments Δ_u are derived. The PDFs show significant deviations from a Gaussian distribution with longer tails typical for an intermittent flow. Local energy dissipation rates ε_τ are derived from subsequences with a duration of $\tau = 1$ s. With a mean horizontal wind velocity of 8 m s^{-1}, τ corresponds to a spatial scale of 8 m. The PDFs of ε_τ can be well approximated with a lognormal distribution that agrees with classical theory. Maximum values of $\varepsilon_\tau \approx 10^{-1}$ m^2 s^{-3} are found in the analyzed clouds. The consequences of this wide range of ε_τ values for particle–turbulence interaction are discussed.

1. Introduction

The question of how atmospheric turbulence impacts cloud microphysical properties and cloud evolution has benefited from renewed interest in the past several years with many recent advances summarized by Shaw (2003) and Vaillancourt and Yau (2000). Long-lived vortex tubes on spatial scales close to the Kolmogorov microscale (which typically is ~1 mm or so) have been hypothesized to cause preferential concentration of droplets and supersaturation intermittency (e.g., Shaw et al. 1998; Shaw 2000), thereby promoting the growths of "favored" droplets and the onset of active coalescence. The ability of turbulence to enhance droplet collision rates has also been demonstrated to be effective at relatively low Reynolds numbers (Vohl et al. 1999; Shaw 2003; Pinsky and Khain 2004), thus raising the question of the efficiency of these processes in real clouds. Recent studies have also begun to look at the effect of the cloud microphysical structure on the statistics of the turbulent flow field. The modification of the turbulent energy spectrum by solid particles with diameters smaller than the Kolmogorov microscale was investigated with direct numerical simulation (DNS) methods by Ferrante and Elgobashi (2003) and Elgobashi and Truesdell (1993). They found that solid particles increase the fluid turbulence energy at high wavenumbers. The influence of water droplets in a multiphase flow proves to be a more challenging problem, in large part because the evaporation or condensation of vapor from or onto droplets strongly affects the local buoyancy. However, because of the small volume and mass fraction the impact of cloud droplets on the flow is supposed to be negligible (Vaillancourt and Yau 2000).

One of the first airborne measurements of vertical wind velocities in clouds was presented in Telford and Warner (1962) indicating a significant increase of turbulence within clouds. The first power spectral densities $S(f)$ of the liquid water content (LWC) were shown in Ackerman (1967) with a resolution of better than

Corresponding author address: Holger Siebert, Leibniz-Institute for Tropospheric Research, Permoserstr. 15, 04318 Leipzig, Germany.
E-mail: siebert@tropos.de

100 m. MacPherson and Isaac (1977) presented the first airborne measurements of $S(f)$ of all three wind velocity components in cumulus clouds and estimated a mean energy dissipation rate of $\bar{\varepsilon} = 0.16\ \mathrm{m^2\,s^{-3}}$ near cloud top. The horizontal resolution of the wind velocity measurements was about 15 m at a true airspeed (TAS) of the aircraft of 130 $\mathrm{m\,s^{-1}}$. More recent airborne measurements of turbulence in stratiform clouds are described in Nicholls (1984), Nicholls and Leighton (1986), and Lenschow et al. (2000); while Smith and Jonas (1995) describe $S(f)$ of the vertical wind velocity component and energy dissipation rates in small cumulus clouds. However, our knowledge of turbulence in clouds is confined to scales much larger than the scales at which interactions between microphysics and turbulence take place.

Today, single droplet measurements on the millimeter scale using the Forward Scattering Spectrometer Probe (FSSP), Fast-FSSP (Brenguier 1993; Brenguier et al. 1998), and the modified Fast-FSSP (M-Fast FSSP; Schmidt et al. 2004) are available. Airborne data of the LWC with the Particle Volume Monitor (PVM-100A; Gerber et al. 2001) and of static air temperature in clouds using the ultrafast thermometers (UFT; Haman et al. 2001) are also on-hand and deliver data with centimeter resolution. Vaillancourt and Yau (2000) pointed out that turbulence measurements with much higher resolution (than several meters) would be needed to investigate the intermittent structure of clouds. Furthermore, all the discussions concerning droplet–turbulence interaction are based on the assumption that turbulence in clouds can be described with the same methods as turbulence in a droplet-free flow. However, the validity of this hypothesis has only been established for spatial scales on the order of several meters since in situ measurements of the turbulent velocity field in clouds with higher resolution were simply not available so far (see discussion in Vaillancourt and Yau 2000).

To overcome the limited spatial resolution (due to typically high TAS of research aircraft) slower-flying helicopters (e.g., Muschinski et al. 2001) have been used yielding spatial resolutions of the measurements below one meter. Tethered balloons have also been used to further increase the spatial resolution. Such balloon measurements were reported by Muschinski et al. (2004), who estimated local ε values and temperature structure parameters. These measurements were based on fine-wire sensors, which are difficult to use under cloudy conditions. Other balloon-borne measurements were reported by Gerber (1986), Blanc et al. (1989), and Plant et al. (1998). These measurements did not include high-resolution turbulence sensors. Tethered balloon–borne turbulence measurements in small cumulus clouds were reported by Kitchen and Caughey (1981), where power spectral densities of the vertical wind at frequencies up to 5 Hz were reported.

To investigate the spatial structure of turbulence in clouds on smaller scales, Siebert et al. (2003) developed the tethered balloon–borne payload Airborne Cloud Turbulence Observation System (ACTOS). The spatial resolution that can be achieved with the measurements of ACTOS (wind vector components, temperature, and LWC) is in the order of 10 cm, which is the highest possible resolution so far.

The main objective of this work is to test the hypothesis that basic ideas of classical turbulence theory (Kolmogorov 1941, 1962; Oboukhov 1962; Batchelor 1953) in boundary layer clouds are valid even to the decimeter scale. For this purpose, two datasets with measurements in different types of boundary layer clouds are analyzed. For temperature measurements in clouds this hypothesis has already been discussed (e.g., Haman et al. 2001), therefore, here we focus on high-resolution wind velocity measurements.

After a brief overview of the instrumental setup (section 2), the two datasets used in this study are introduced (section 3). In section 4 the structure of the turbulent flow, down to centimeter scales, is explored in more detail, with a particular emphasis on local (8 m) estimates of ε and the associated pdfs of the wind.

2. Instrumentation

High-frequency measurements of the three-dimensional wind vector in boundary layer clouds were made with ACTOS carried by the tethered balloon Mobiles Autonomes Positionierungs System (MAPS-Y; Siebert et al. 2003). ACTOS is an instrumental payload that, in addition to measuring the three-dimensional wind vector, also measures static temperature, and humidity each with a sampling frequency of at least 100 Hz. A PVM-100A (Gerber 1991; Gerber et al. 1994) measures the LWC; cloud droplet size distributions are derived from measurements with the M-Fast-FSSP. A photo of the current version of ACTOS is shown in Fig. 1. ACTOS consists of four shielded 19-in racks that include power supply, real-time data acquisition, and further sensor electronics. The turbulence sensors are fixed to a 1.5-m-long outrigger made of lightweight carbon fiber. Two tail units keep ACTOS aligned with the mean wind. A navigation unit including a differential global positioning system (GPS), an inertial navigation system (INS), and a high-resolution barometer allows recon-

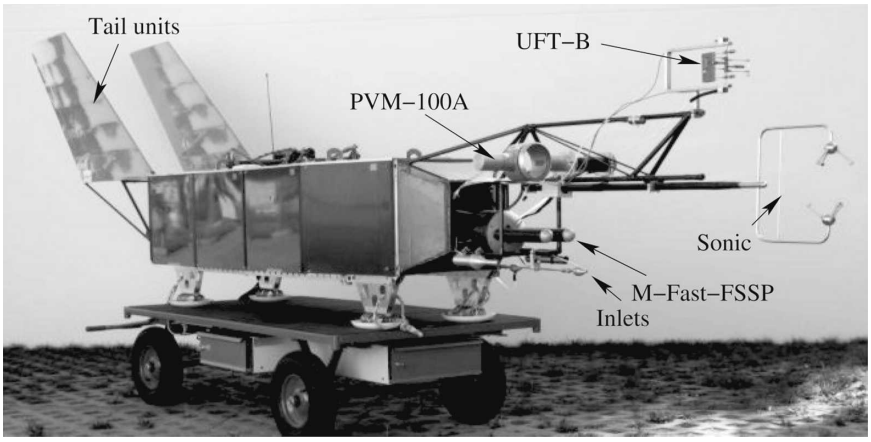

FIG. 1. The turbulence payload ACTOS with sonic, UFT-B, PVM-100A, and M-Fast-FSSP. Also shown are the inlets for humidity and aerosol particle measurements.

struction of the ACTOS attitude, position, and motion. The total mass of ACTOS is 120 kg.

This work is mainly based on data from the ultrasonic anemometer (hereafter called sonic) and the navigation unit. The LWC and the static air temperature measured with a shielded fine-wire resistance thermometer (UFT-B; Haman et al. 2000) are used to give an overview of the general conditions only.

a. Sonic measurement

The sonic used in this study is a three-dimensional Solent-Research Horizontally Symmetric (HS), manufactured by Gill Instruments, Lymington, United Kingdom. The maximum sampling frequency is 100 Hz; that is, the Nyquist frequency f_{Ny} is 50 Hz. From laboratory investigations (Siebert and Muschinski 2001) the spectral noise floor $S_{u_i}^{(n)}$ for u_i ($i = 1$, 2, and 3 for the three wind velocity components) is estimated to about 10^{-5} $\mathrm{m^2\,s^{-2}\,Hz^{-1}}$, the standard deviation due to uncorrelated noise is $\sigma_{u_i}^{(n)} = \sqrt{S_{u_i}^{(n)} f_{\mathrm{Ny}}} \approx 2\ \mathrm{cm\,s^{-1}}$. The sensitive pathlength for the measurements is 15 cm for all three wind velocity components, which determines the spatial resolution of the sonic (Kaimal et al. 1968). The sonic was fixed at the tip of the outrigger to minimize flow distortions induced by the body of ACTOS. The distance between sonic and the closed 19-inch racks of ACTOS is 1.5 m, which is 3 times the width of ACTOS (cf. Fig. 1). For in-cloud measurements with sonics, the wind data have been found to be unbiased by water droplets (Siebert and Teichmann 2000).

b. Corrections for payload attitude and motion

The measurements of the wind vector with the sonic refer to a payload-fixed coordinate system and, therefore, have to be corrected for attitude and motion of ACTOS. The correction has been performed following Lenschow (1986) and Edson et al. (1998).

In the standard configuration of ACTOS, the roll and pitch angles are directly derived from the INS data. The GPS system (TANS Vector, Trimble Ltd., Sunnyvale, California) is a multiantenna array that measures all three attitude angles using differential carrier phase measurements between the four antennas. Only the heading is used to support the INS in the low frequency range. The resolution of roll and pitch from the INS is about 0.0006° and 0.2° for the heading (including stabilization with GPS heading). The measure of the translational velocity vector of ACTOS is also a combination of INS and GPS data.

The three attitude angles can also be derived directly from the GPS, though with lower resolution (0.3° for roll and pitch and 0.2° for the heading angles). In this case, the wind measurements can only be corrected for attitude since the accuracy and data availability of the translational velocity components from the GPS is incomplete. Therefore, calculated wind velocity data show a peak around the pendulum frequency at 0.1 Hz, most significant for the lateral wind component. Only high-pass-filtered data with a cutoff frequency >0.1 Hz can then be used for further analysis.

c. ACTOS and MAPS-Y

ACTOS is lifted with the tethered balloon MAPS-Y up to a height of around 1.5 km depending on wind conditions. The maximum wind speed for the system is $15\ \mathrm{m\,s^{-1}}$. MAPS-Y has a volume of $400\ \mathrm{m^3}$ and can be filled either with hydrogen or helium. The maximum climbing rate is around $1.5\ \mathrm{m\,s^{-1}}$ for moderate wind speeds and up to $3\ \mathrm{m\,s^{-1}}$ for wind speeds below $5\ \mathrm{m\,s^{-1}}$.

The payload was fixed 25 m below MAPS-Y to overcome the influence of flow distortions induced by the balloon itself (cf. Wills and Cole 1986). More details and a photo of MAPS-Y can be found in Siebert et al. (2003).

3. Data overview

In this work data from two field campaigns are considered. The first experiment was the Baltex Bridge Campaign (BBC2; Crewell et al. 2004), which was conducted near Cabauw, Netherlands, in May 2003. The second was called Influence of Clouds on Spectral Actinic Flux in the Lower Troposphere (INSPECTRO2) and took place in southern Germany in May 2004. From both campaigns, a time series recorded during constant level flights is analyzed. Measurements of the attitude-corrected longitudinal wind velocity U, vertical velocity W, static air temperature T_a, and LWC are presented. Actual values are indicated by capitals, whereas the fluctuating part is described by lower case letters: $X(t) = \overline{X} + x(t)$. An overbar represents an average over the complete record.

a. BBC2 campaign

A 20-min-long record taken on 21 May 2003 between 0947 and 1006 UTC was analyzed in detail. More than 50% of the flight time was in clouds. The flight height was 760 ± 20 m. Shallow cumulus clouds (Cu med) were observed by a horizontal-looking video camera onboard ACTOS. The cloud base was around 500 m as estimated from a ground-based ceilometer (CT 75, Vaisala, Finland). Figure 2 shows two vertical profiles of static air temperature T_a, relative humidity RH, horizontal wind speed U, and wind direction D as derived from radiosonde data (soundings from 0830 and 1121 UTC). The temperature at cloud base was 8°C as derived from Fig. 2. A small temperature inversion with a significant decrease of relative humidity was observed in the first profile around 1200-m altitude in association with cloud top. However, the picture given by the two soundings is not completely consistent. In particular, the relative humidity profiles differ significantly, which is most likely caused by the local cloud situation for the individual sounding. In the measurement height of ACTOS (marked with a horizontal line in Fig. 2), no significant temperature inversion or change in the wind direction happened in between the soundings. It was not possible to measure meaningful vertical profiles in clouds with ACTOS because of the limited horizontal extension of the clouds.

Figure 3 shows the time series of U, W, LWC, and T_a measured with ACTOS. During this flight, the INS was not running because of a technical problem; therefore, the wind velocity components were corrected for roll and pitch angle derived from GPS. In Fig. 3 both wind components are low-pass filtered (second-order Butterworth, $f_{\text{cut}} = 0.05$ Hz) to reduce the oscillation due to the pendulum motion. The mean horizontal wind was $\overline{U} = 8.1$ m s^{-1} with maxima around 12 m s^{-1} in the clouds. The standard deviation σ of the longitudinal and vertical wind velocity component was 1.2 m s^{-1}, most positive vertical velocities were measured within the clouds. The mean temperature was 6.3°C with $\sigma_{T_a} =$ 0.2 K for the complete record. A decrease of T_a was observed at cloud edges, highest temperatures were observed inside the clouds. This behavior can be explained by vertical updrafts in clouds (positive W) with warmer air from lower levels. At cloud edges a downward motion dominated together with evaporative cooling. This suggests that the observed clouds are still in a stage of development. The mean LWC at this flight level was 0.45 g m^{-3}. Maximum values 0.5 g m^{-3} coincides with the adiabatic LWC value assuming the cloud base in 500 m height.

b. INSPECTRO2 campaign

From the INSPECTRO2 campaign a time series from the 16 May 2004 is analyzed (cf. Fig. 4). This record is 33 min long and was also taken at a nearly constant altitude of 1540 ± 40 m. The sky was covered with a layer of scattered shallow fair weather cumuli (Cu humilis), which run flat and disappeared shortly after these measurements. Using the onboard camera, the position of ACTOS was estimated to be in the lower third of the clouds.

During this period the navigation unit worked properly and, therefore, the wind vector was completely corrected for attitude and translational motion as described in section 2b. The mean horizontal wind was 7.4 m s^{-1} ($\sigma_U = 1.4$ m s^{-1}). The vertical wind velocity showed strong fluctuations with positive and negative values outside the cloud, whereas inside the cloud W was almost always positive. A few small cloud holes corresponded well with downdrafts. After the cloud section W fluctuated around zero with an amplitude of about 1 m s^{-1}. The temperature was near zero with lowest values of around −1°C.

The structure of the LWC field was very inhomogeneous even inside the cloud. A 100-s-long subsequence of the LWC time series is enlarged at the top panel of Fig. 4. Part A of this subsequence shows a more homogeneous LWC field, whereas part B exhibits more fluctuations of the LWC. These clouds are much less dy-

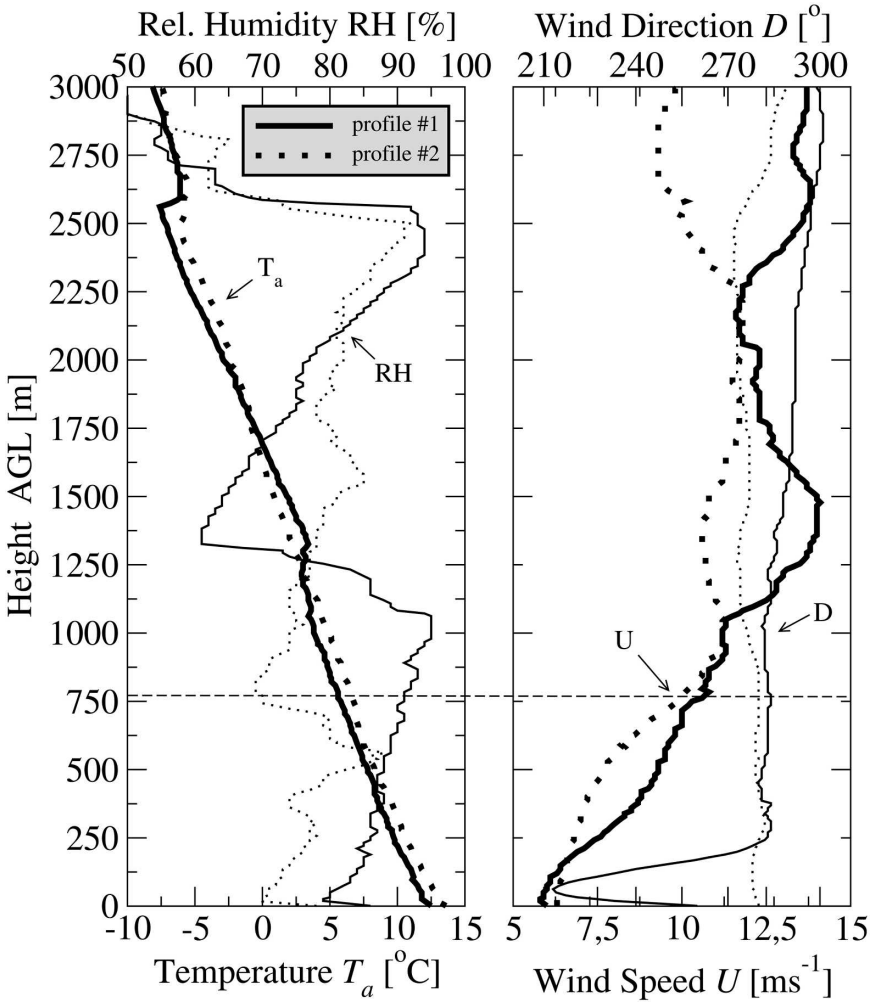

FIG. 2. Two vertical profiles of (left) air temperature (T_a) and RH and (right) horizontal wind speed (U) and wind direction (D). The profiles were derived from radiosondes that were launched close to the balloon site. The first radiosonde was launched at 0830 UTC, the second at 1121 UTC. A horizontal line marks the height of the balloon between 0947 and 1006 UTC.

namic compared with the BBC2 clouds and are in the stage of decaying.

4. Data analysis

a. *Spectral analysis and mean energy dissipation rates* $\bar{\varepsilon}$

Assuming local isotropy and stationarity of the turbulence (e.g., Batchelor 1953), in the wavenumber domain the power spectral density $F(k)$ in the inertial subrange is given by

$$F(k) = \alpha \bar{\varepsilon}^{2/3} k^{-5/3}, \tag{1}$$

with the wavenumber k, the mean energy dissipation rate $\bar{\varepsilon}$, and the one-dimensional Kolmogorov constant $\alpha \approx 0.5$ for the streamwise velocity component u. The power spectral density $S(f)$ in the frequency domain can be related to $F(k)$ using the Taylor hypothesis ($k = 2\pi f/\overline{U}$) as follows:

$$S(f) = \frac{2\pi}{\overline{U}} F(k) = \alpha \bar{\varepsilon}^{2/3} \left(\frac{\overline{U}}{2\pi}\right)^{2/3} f^{-5/3}. \tag{2}$$

With $S(f)$ measured in the inertial subrange, $\bar{\varepsilon}$ can be estimated as

$$\bar{\varepsilon} = \frac{2\pi}{\overline{U}} \left(\frac{f^{5/3} S(f)}{\alpha}\right)^{3/2}. \tag{3}$$

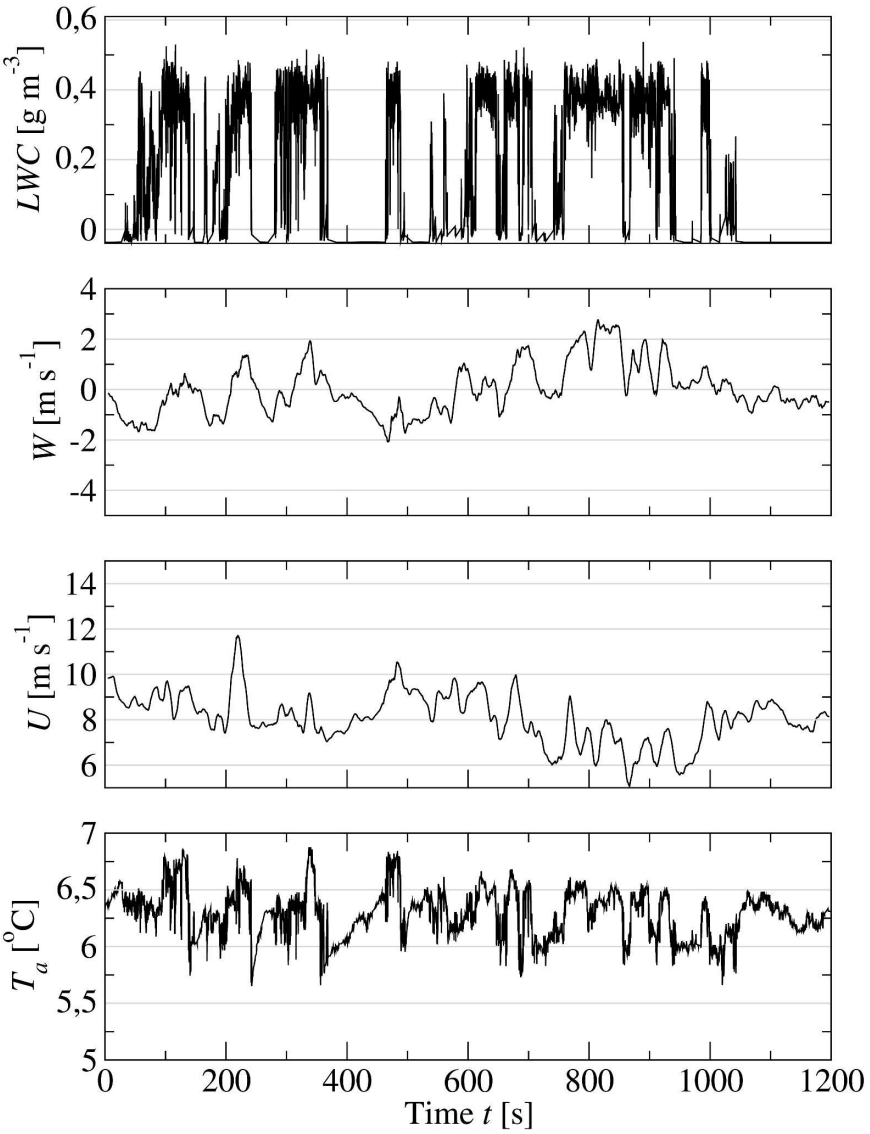

FIG. 3. Time series of LWC, vertical wind velocity W, horizontal wind velocity U, and temperature T_a as measured with ACTOS at a height of around 760 m AGL on 21 May 2003 during the BBC2 campaign.

This method is called the inertial dissipation method (Champagne et al. 1977; Oncley et al. 1996).

The records of both datasets were analyzed with one-dimensional power spectral densities $S(f)$ to estimate the mean energy dissipation rate and to verify a $-5/3$ slope as an indication for inertial subrange behavior. Before using a Fast Fourier Transformation (FFT) routine, a Hanning window was applied. The one-sided spectra of quantity $x(t)$ are related to the corresponding variance σ_x^2 through

$$\sigma_x^2 = \int_0^\infty S_x(f)\, df. \tag{4}$$

All raw spectra were averaged over equidistant logarithmic frequency bins, eight bins per decade were chosen as suggested by Kaimal and Finnigan (1994). An $f^{-5/3}$ fit is given for inertial subrange behavior. Using the Taylor hypothesis $\overline{U} = \lambda f$, the frequencies are converted into the wavelengths λ with the mean horizontal wind speed (assuming a value of $\overline{U} = 8$ m s^{-1} for both records). The Taylor hypothesis is assumed to be valid when the turbulence intensity $I \equiv \sigma_u/\overline{U}$ is smaller than 0.5 (Willis and Deardorff 1976), which is satisfied for the presented data and with the values given in Table 1.

Figure 5 shows $S(f)$ for all parameters presented in Figs. 3 and 4 (LWC, W, U, T_a). All $S(f)$ of the BBC2

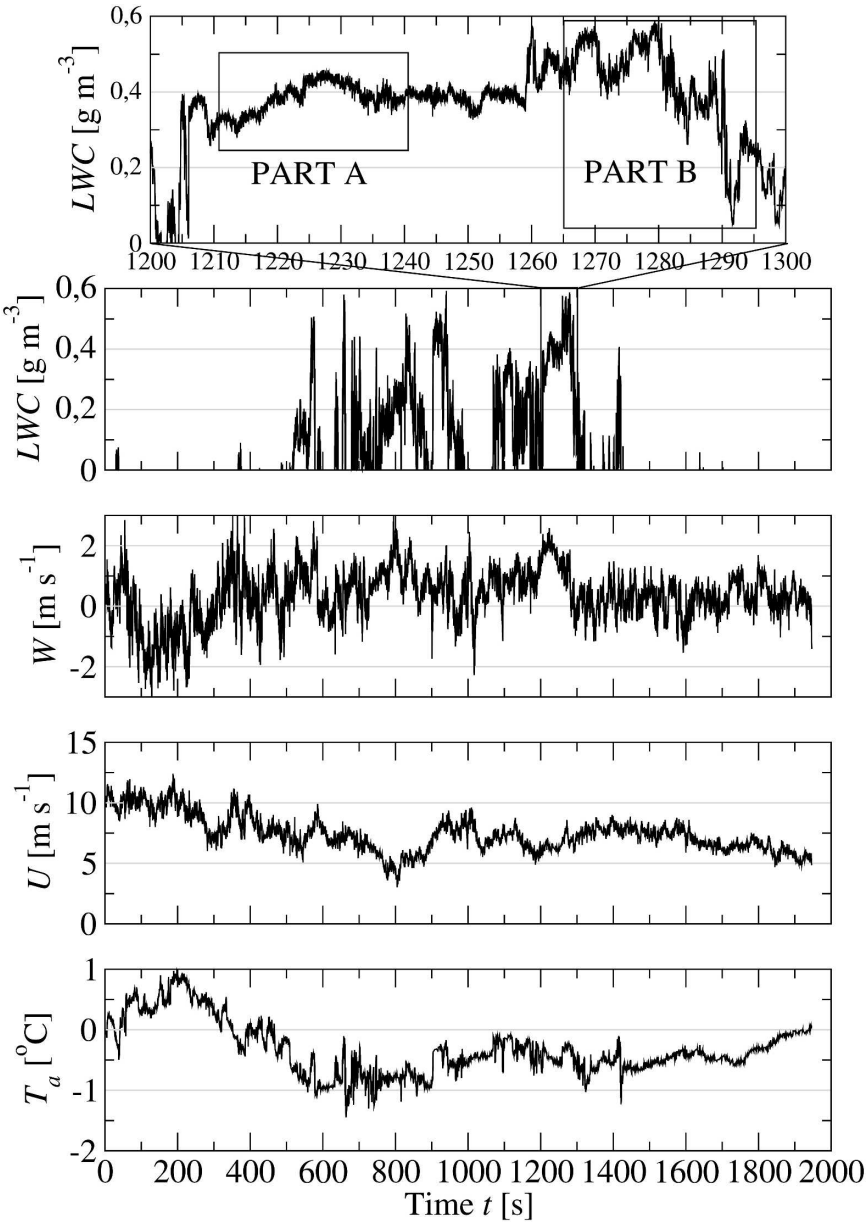

FIG. 4. Time series of LWC, vertical wind velocity W, horizontal wind velocity U, and temperature T_a as measured with ACTOS at a height of around 1540 m AGL on 16 May 2004 during the INSPECTRO campaign.

data are divided by a factor of 10 to clearly distinguish from INSPECTRO2 data. For frequencies higher 0.1 Hz all spectra closely follow a −5/3 slope. The spectra of u and w for the BBC2 data show a slight peak around 0.1 Hz due to the pendulum motion that could not completely be removed. The $S(f)$ of both velocity components of the INSPECTRO2 data show a slight flattening for frequencies higher 30 Hz. This behavior was

TABLE 1. Statistical parameters of the complete time series shown in Figs. 3 and 4.

	$\overline{U}$ (m s^{-1})	σ_U^2 (m^2 s^{-2})	σ_W^2 (m^2 s^{-2})	$\overline{T}$ (°C)	σ_T^2 (K^2)	$\overline{\varepsilon}$ (m^2 s^{-3})
BBC2	8.1	1.5	1.33	6.3	0.04	3×10^{-3}
INSPECTR02	7.4	2.0	0.68	−0.2	0.24	2×10^{-3}

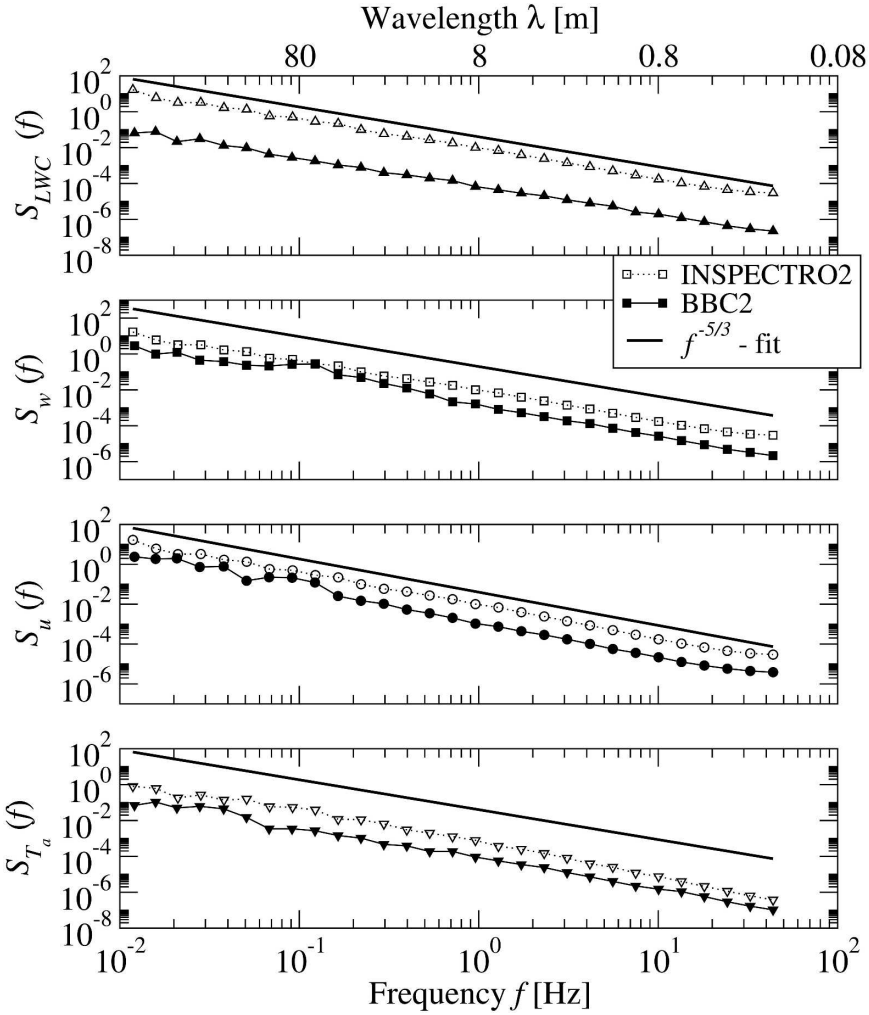

FIG. 5. Power spectral densities $S(f)$ of the same data as presented in Figs. 3 and 4. All spectra are in units of their variance per frequency; spectra of BBC data are divided by a factor of 10 for better resolution. For the top panel the frequencies are converted into wavelength assuming a constant horizontal wind speed of 8 m s^{-1}.

observed with the same type of sonic during a previous ground-based experiment (Siebert and Muschinski 2001).

With Eq. (3), $\bar{\varepsilon} = 3 \times 10^{-3}$ m^2 s^{-3} for the BBC2 data and $\bar{\varepsilon} = 2 \times 10^{-3}$ m^2 s^{-3} for the INSPECTRO2 data are estimated. The Taylor's Reynolds number

$$\mathrm{Re}_\lambda = \sigma_u \lambda_T / \nu = \sigma_u^2 \sqrt{15/(\nu\bar{\varepsilon})} \tag{5}$$

with the Taylor microscale $\lambda_T = \sigma_u \sqrt{15\nu/\bar{\varepsilon}}$ and the kinematic viscosity $\nu = 1.5 \times 10^{-5}$ m^2 s^{-1} is estimated to $\mathrm{Re}_\lambda \approx 3 - 4 \times 10^4$ for both datasets which is significantly higher than the critical value of 500, which means a high Reynolds number flow, and therefore fully developed turbulence (cf. Frehlich et al. 2004). The mean values and variances of all parameters are summarized for both records (BBC2 and INSPECTRO2) in Table 1.

b. Local isotropy

The classical turbulence theory of Kolmogorov (1941) in the inertial subrange is based on the assumption of local isotropic conditions. This theory predicts a 4/3 ratio between the $S(f)$ of lateral and longitudinal wind velocity components in the inertial subrange (Kaimal et al. 1972):

$$\frac{S_v}{S_u} = \frac{S_w}{S_u} = \frac{4}{3}. \tag{6}$$

Figure 6 shows the spectral ratios for the BBC2 data (top) and the INSPECTRO2 data (bottom) in the frequency range between 1 and 50 Hz. The lower boundary is chosen to exclude data influenced by the pendulum motion of the system while the higher boundary is

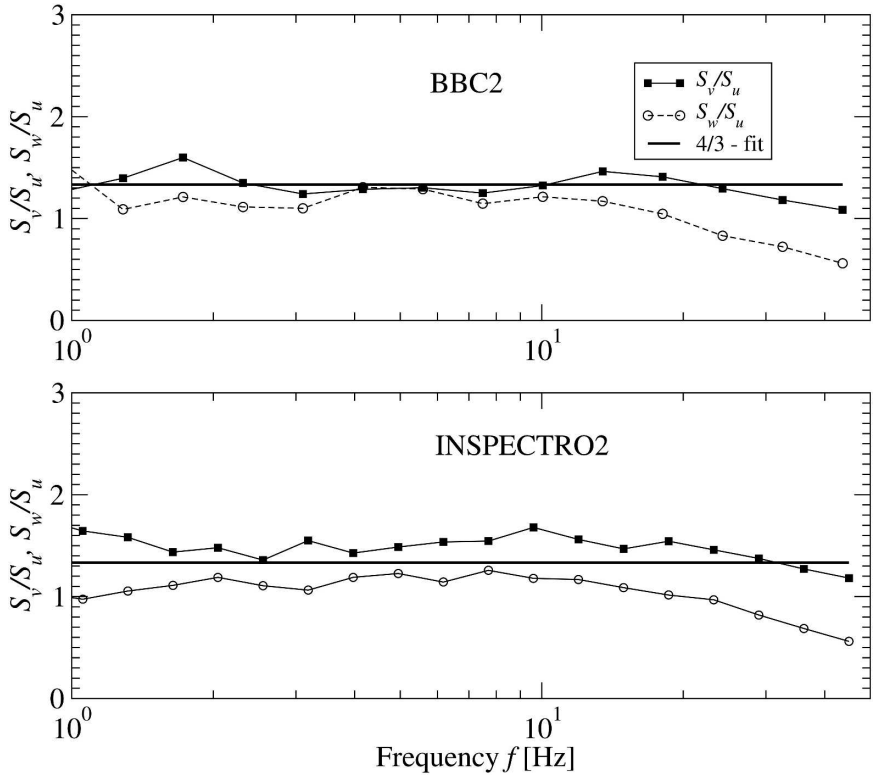

FIG. 6. Spectral ratios S_v/S_u and S_w/S_u for (top) BBC2 data and (bottom) INSPECTRO2 data. A 4/3 ratio is plotted for reference, indicating the value predicted by classical theory for isotropic turbulence.

determined by the Nyquist frequency. In general, all measured ratios exhibit some scatter but are closer to 4/3 than to unity indicating local isotropy over this range. One possible reason for the observed scatter in the ratios of $S(f)$ might be the occurrence of shear and buoyancy, which might violate the assumption of local isotropy (Saddoughi and Veeravalli 1994; Biltoft 2001). For the BBC2 data, both ratios are close to 4/3 up to 20 Hz (S_v/S_u) and 10 Hz (S_w/S_u), respectively. For higher frequencies the ratios significantly drop below one. This corresponds to the slight flattening of S_u and different spectral transfer functions of the sonic for different velocity components close to the Nyquist frequency. For the INSPECTRO2 data the behavior is similar to BBC2. However, S_v/S_u is always higher than 4/3 whereas S_w/S_u is always below 4/3 before both ratios drop off.

c. Local energy dissipation rates

The small-scale structure of the turbulence is investigated by means of so-called local energy dissipation rates ε_τ where the index τ indicates the averaging time over which the parameter is estimated. In this context, based on the work by Kolmogorov (1962) and Oboukhov (1962), ε_τ is used as a random variable compared to $\bar{\varepsilon}$, which is obtained from the complete time series [see Eq. (3)]. It should be pointed out that the value of ε_τ depends on τ, that is, $\varepsilon_{\tau_1} \neq \varepsilon_{\tau_2}$ for $\tau_1 \neq \tau_2$ and $\varepsilon_\tau \Rightarrow \bar{\varepsilon}$ for τ converges to the length of the record. Typical values of τ as derived from airborne measurements are on the order of seconds (Frehlich et al. 2004; Muschinski et al. 2004), which is much longer than the time resolution needed to resolve the Kolmogorov length scale. In this work, $\tau = 1$ s is chosen since this is the smallest time for a stable estimation of an inertial subrange under most conditions. However, it has to be pointed out that this value of τ is somewhat arbitrary. A detailed discussion of local energy dissipation measurements in the atmosphere can be found in Muschinski et al. (2004). Here, only a few different techniques to derive local energy dissipation rates are discussed:

(i) the inertial dissipation method based on Eq. (3), which was applied to the complete record to estimate $\bar{\varepsilon}$ can be used with shorter averaging times τ to estimate ε_τ;
(ii) the direct method based on the definition of ε (lo-

cal isotropy and the validity of Taylor's hypothesis are assumed):

$$\varepsilon_\tau \equiv \frac{15\nu}{\langle U\rangle_\tau^2}\langle(\partial_t u)^2\rangle_\tau. \tag{7}$$

Here, $\langle x\rangle_\tau$ indicates an average of x over the time τ. The direct method requires measurements with a spatial resolution in the order of the Kolmogorov length scale of ~1 mm (Oncley et al. 1996; Champagne et al. 1977), which is not possible with sonics.

(iii) The relation between the variance and $S(f)$ [cf. Eq. (4)] can be solved for the case that the complete frequency range is within the inertial subrange:

$$\sigma_u^2 = \langle u^2\rangle_\tau = \int_0^\infty \alpha\varepsilon_\tau^{2/3}\left(\frac{\langle U\rangle_\tau}{2\pi}\right)^{2/3} f^{-5/3}\,df$$

$$\approx \alpha\varepsilon_\tau^{2/3}\left(\frac{\langle U\rangle_\tau}{2\pi}\right)^{2/3} f_0^{-2/3}, \tag{8}$$

in the frequency interval $[f_0; f_{\mathrm{Ny}}]$ and $f_0 \ll f_{\mathrm{Ny}}$:

$$\varepsilon_\tau = \frac{2\pi}{\langle U\rangle_\tau}\frac{f_0}{\alpha^{3/2}}\langle u^2\rangle_\tau^{3/2}, \tag{9}$$

with $f_0 = 1/T_0 = 1/(2T)$; and, finally

(iv) ε_τ can be derived from the second-order structure parameter $(C_u^2)_\tau = 2\varepsilon_\tau^{2/3}$ of u:

$$D_u^\tau(t') = (C_u^2)_\tau(t'\langle U\rangle_\tau)^{2/3}$$

$$= 2\varepsilon_\tau^{2/3}(t'\langle U\rangle_\tau)^{2/3}, \tag{10}$$

and, therefore,

$$\varepsilon_\tau = (0.5D_u^\tau(t'))^{3/2}/(t'\langle U\rangle_\tau) \tag{11}$$

with the second-order structure function $D_u^\tau(t') = \langle(u(t+t') - u(t))^2\rangle_\tau$ and the time lag t'.

Figure 7 shows a correlation plot of ε_τ estimated with the three different methods. Here, the local energy dissipation rate derived from $S(f)$ in the inertial subrange is indicated with ε_{S_u}, the dissipation rate derived from the structure function has the index C_u^2, and the energy dissipation rate proportional to σ_u^3 has the index σ^3, respectively. In the lower panel of Fig. 7 a short time series of ε_{σ^3}, $\varepsilon_{C_u^2}$, and ε_{S_u} is shown. In general all methods are useful to describe the local structure of ε_τ on such small scales. However, the inertial subrange method sometimes underestimates ε_τ at low values (cf. negative peak at $t = 47$ s). In such cases no clear inertial subrange behavior was observed in $S(f)$ except in the structure function. Therefore, the method using the second-order structure parameter is, however, more robust for cases with small values of ε_τ. One reason for this behavior might be that this method does not need any additional windowing or other data conditioning that has significant influence on $S(f)$ of such short time series. The mean differences between ε_{σ^3} and $\varepsilon_{C_u^2}$ are in the order of 2 and, therefore, negligible. For further analysis, the method using the second-order structure parameter is used, the index C_u^2 is left out for simplification. The following statistical analysis of ε_τ was made for all three methods without any significant differences.

In Fig. 8 the time series of the local ε_τ is presented for BBC2 data. Additionally, a running average over 10 points is included. The values of local ε_τ cover a range of nearly four orders of magnitude.

For the BBC2 data, minimum values of ε_τ down to 10^{-5} m^2 s^{-3} were found in the cloud-free areas, absolute minima are often found just outside the clouds (cf. marked regions i and ii in Fig. 8). The mean value is $\bar{\varepsilon}_\tau = 6 \times 10^{-3}$ m^2 s^{-3} with $\sigma_{\varepsilon_\tau} = 2 \times 10^{-2}$ m^2 s^{-3}. Maximum values of ε_τ around 0.1 m^2 s^{-3} are found inside of clouds, for example the single cloud labeled iii in Fig. 8. The gradient of ε_τ can be very high around cloud edges; for example, the distance between local maxima of ε_τ just at the cloud edge around $t = 237$ s and the local minima in the cloud-free region at $t = 243$ s is within 50-m horizontal distance where ε_τ decreases by nearly four orders of magnitude.

The relation between the standard deviation $\sigma_{\varepsilon_\tau}$ and $\bar{\varepsilon}_\tau$ depends on Re_λ and can be approximated by (e.g., Pope 2000):

$$\sigma_{\varepsilon_\tau} = \sqrt{\mathrm{Re}_\lambda^{3/8}\varepsilon_\tau^{-2}}. \tag{12}$$

With $\mathrm{Re}_\lambda = 4 \times 10^4$ and $\bar{\varepsilon}_\tau$ given above, Eq. (12) results in $\sigma_{\varepsilon_\tau} \approx 4 \times 10^{-2}$ m^2 s^{-3}, which is in good agreement with 2×10^{-2} m^2 s^{-3} directly derived from the time series of ε_τ.

For the INSPECTRO2 data (Fig. 9) the correlation between local ε_τ and LWC was not as obvious. The smallest values were found inside homogeneous parts of clouds, such as part A. Higher values were found in regions of high fluctuations of LWC, especially at cloud edges (see, e.g., dashed box), where lateral entrainment of dry air created stronger fluctuations due to evaporative cooling.

d. PDFs of wind velocity increments and ε_τ

To analyze the statistics of wind velocity fluctuations in an intermittent flow it is common to calculate the PDFs of the wind velocity increments Δu_i instead of u_i. The increment of a variable $x(t)$ is defined as $\Delta x \equiv x(t+\tau) - x(t)$. Here, the time lag $\tau = 10$ ms is used,

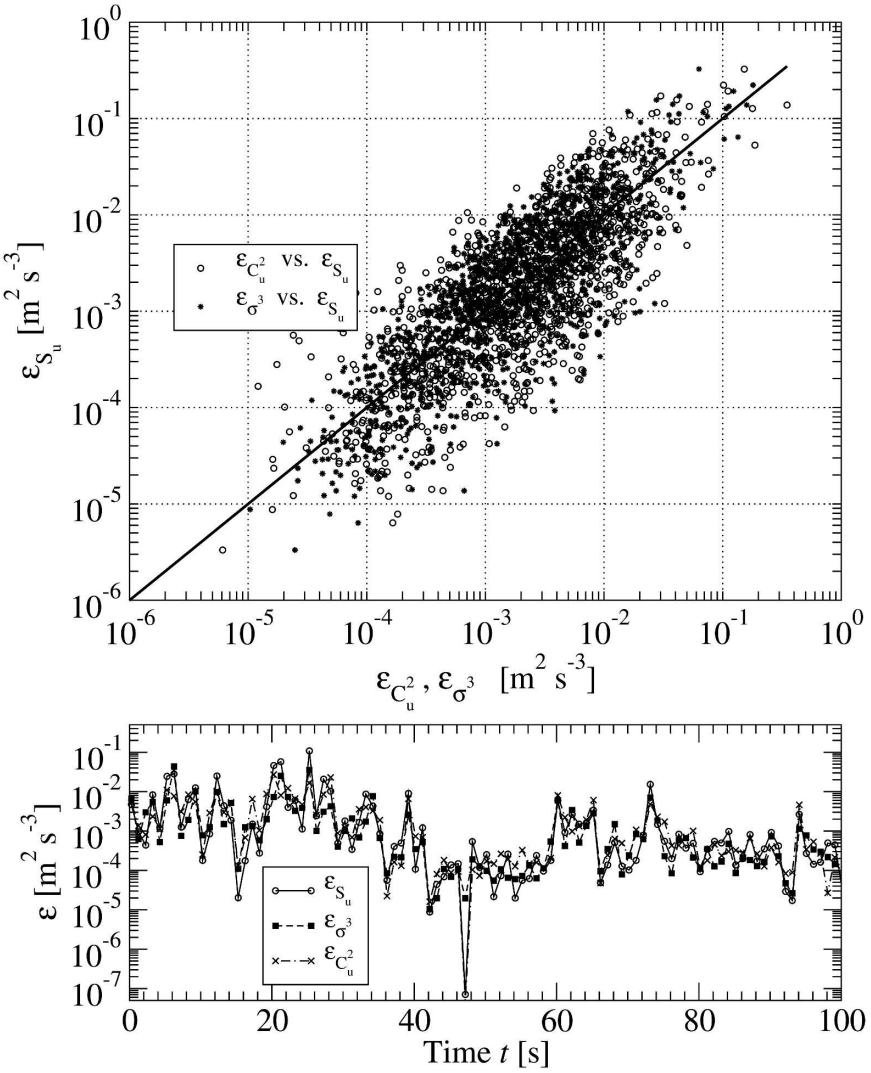

FIG. 7. (top) Correlation of ε_{S_u} vs ε_{σ^3} and $\varepsilon_{C_u^2}$, respectively. Each point represents an ε_τ averaged over a 1-s period ($\tau = 1$ s). (bottom) A short time series of ε_τ calculated with the three methods described in the text.

which is the sampling time of our measurements. In Fig. 10, the PDFs of Δu and Δw for the BBC2 data are presented. To compare these PDFs with model distributions, a Gaussian fit, which is often used as a first-order assumption, is included. All data show a smooth and symmetric PDF, only some scatter can be observed for high absolute values of Δu and Δw. The difference between the Gaussian assumption and the measured PDF is obvious. The shape of the measured PDF is typical for intermittent time series where high values are more frequent than predicted by a Gaussian PDF (Böttcher et al. 2003; Frisch 1995). The probability of the highest values of the measured velocity increments is at least one order of magnitude higher than predicted by a Gaussian distribution that emphasizes the intermittent character of the wind velocity field.

A widely used model assumption for the PDFs of ε_τ in high Reynolds number flows is a lognormal distribution (e.g., Shaw and Oncley 2001). A discussion of different models for PDFs of ε_τ can be found in the review article by Sreenivasan and Antonia (1997). Figure 11 shows the PDFs of the natural logarithm of ε_τ for the BBC2 (top) and INSPECTRO2 (bottom) datasets. Both PDFs are quantitatively well described by a Gaussian distribution; attempts to more quantitatively describe the distributions were hindered by the limited sample.

In Fig. 12 the PDFs of ε_τ conditionally sampled on

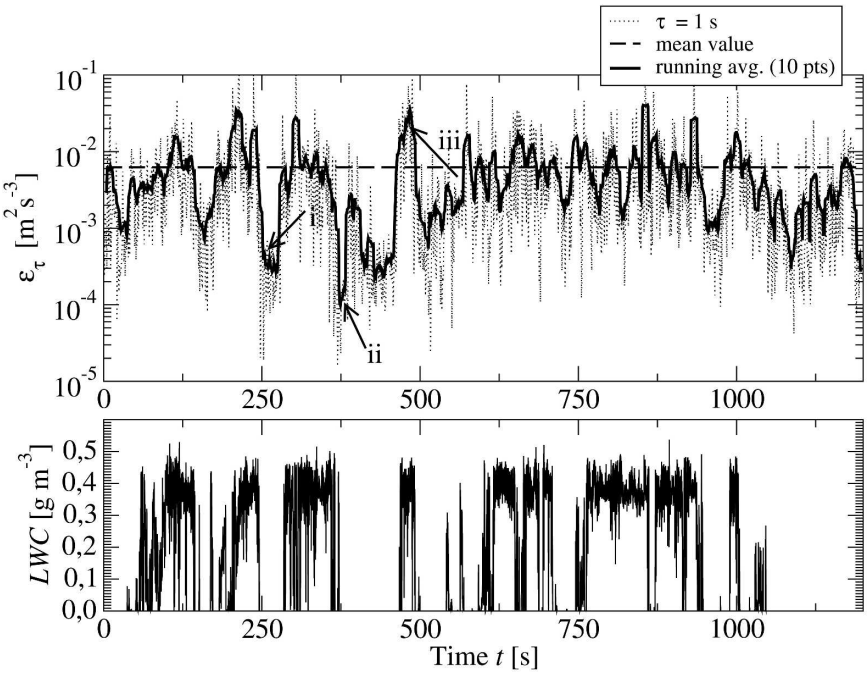

FIG. 8. (top) Time series of local energy dissipation rate ε_τ and (bottom) LWC of BBC2 data. The integration time τ for ε_τ is 1 s; a running average over 10 points is included.

LWC are presented for BBC2 (top) and INSPECTRO2 (bottom) data. In this presentation the differences between the two types of clouds become more evident. For the BBC2 data the PDFs of the cloud and the cloud-free data are clearly shifted to each other. The mean ε_τ inside of clouds is 1×10^{-2} m^2 s^{-3} in contrast to 2×10^{-3} m^2 s^{-3} in the cloud-free regions. A significant increase of the PDF(ε_τ) for cloud-free data coincides with the mean of PDF(ε_τ) for cloud data. This indicates that there are regions associated with updrafts

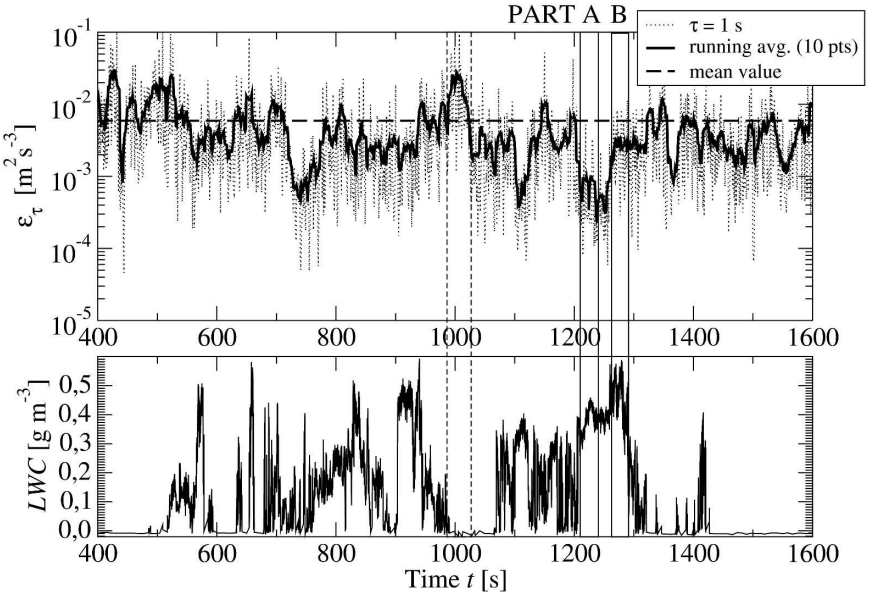

FIG. 9. (top) Time series of local energy dissipation rate ε_τ and (bottom) LWC of INSPECTRO2 data. The integration time τ for ε_τ is 1 s; a running average over 10 points is included.

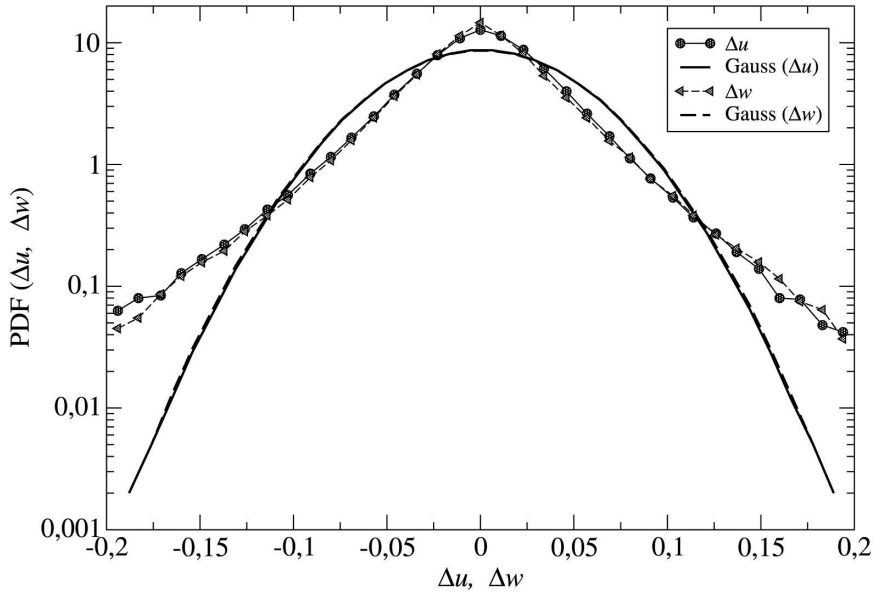

FIG. 10. Semilogarithmic plot of the PDFs of the increments Δu and Δw for the BBC2 data. A Gauss fit is included for reference.

and increased turbulence but not necessarily resulting in clouds. For the INSEPCTRO2 data, this difference is much less obvious (5×10^{-3} m^2 s^{-3} in clouds and 8×10^{-3} m^2 s^{-3} for the cloud-free regions).

5. Discussion

The observed wide range of ε_τ has consequences for the interaction between turbulence and microphysical processes: "The utilization of an averaged value of the dissipation rate can lead to an underestimation of the effects of turbulence on collisions and on precipitation formation. It is quite possible that regions of effective collisions should be well correlated with zones of enhanced turbulence" (Pinsky and Khain 2004).

The key question is whether there are turbulence-induced local accelerations of fluid parcels resulting in different velocities of droplets as a function of their

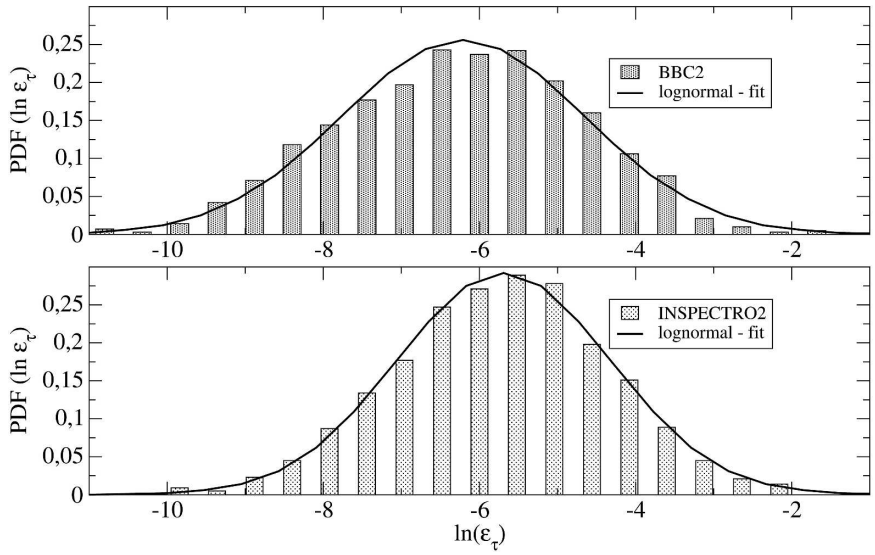

FIG. 11. PDF of natural logarithm of local energy dissipation rates ε_τ. A Gauss fit is included for reference.

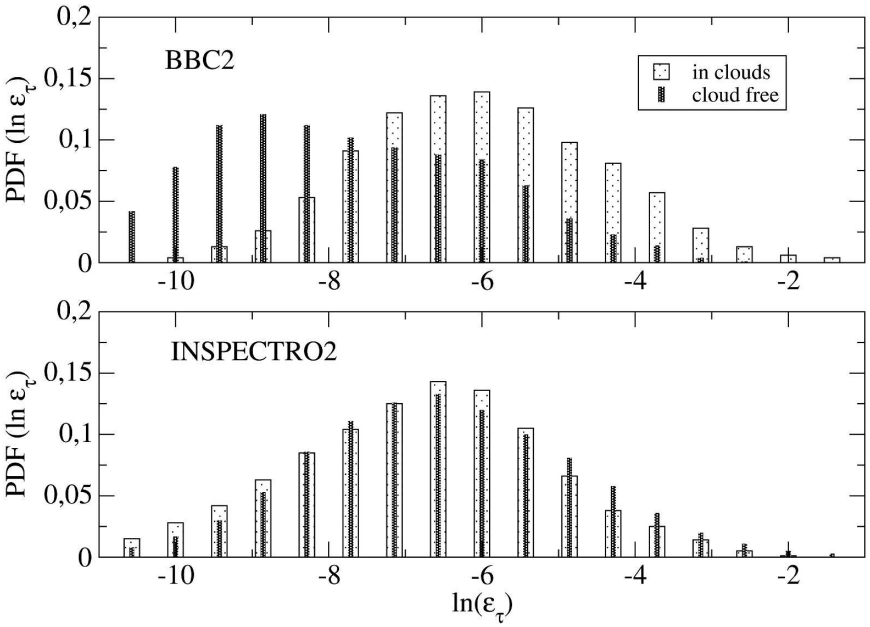

FIG. 12. PDF of natural logarithm of energy dissipation rates of the (top) BBC2 data and (bottom) INSPECTRO2 data inside of clouds and outside of clouds. The energy dissipation rates are conditionally sampled on the LWC.

inertia. Pinsky and Khain (2004) pointed out that "the effect of Lagrangian acceleration is mainly caused by the increase in the collision efficiency that is highly sensitive even to weak variations of interdrop relative velocity."

For this investigation the dimensionless ratio $\langle a_L\rangle_{\rm rms}/g$ with the rms value of the Lagrangian acceleration $\langle a_L\rangle_{\rm rms} = \sqrt{\langle a_L^2\rangle}$ and its intermittent character are most important (Shaw and Oncley 2001). To estimate $\langle a_L\rangle_{\rm rms}$ the expression given by Hill (2002) was used which depends on the Taylor Reynolds number:

$$\langle a_L^2\rangle = \varepsilon^{-3/2}\nu^{-1/2}(2.5{\rm Re}_\lambda^{0.25} + 0.08{\rm Re}_\lambda^{0.11}). \quad (13)$$

For $\bar{\varepsilon}_\tau$ the ratio $\langle a_L\rangle_{\rm rms}/g$ is ≈ 0.2. Averaged over the small cloud marked with iii in Fig. 8 we find a mean energy dissipation rate of $\langle\varepsilon_\tau\rangle_{\rm iii} \approx 0.02\ {\rm m^2\ s^{-3}}$ and ${\rm Re}_\lambda \approx 6000$ ($\sigma_u^2 \approx 0.6\ {\rm m^2\ s^{-2}}$), which yield $\langle a_L\rangle_{\rm rms}/g \approx 0.4$. This is twice the value compared with $\bar{\varepsilon}_\tau$ of the complete record. Pinsky and Khain (2004) estimated an increase of the collision efficiency of 25% with a mean $\bar{\varepsilon} \approx 0.02\ {\rm m^2\ s^{-3}}$ compared to pure gravity acceleration (assuming a droplet collector of $\approx$10 μm in radius).

For this discussion, several points have to be considered. First, the observed clouds are only fair weather clouds and much higher mean and local values of ε can be expected for more convective cumulus clouds. Second, the local ε_τ are averaged over a period τ, which is at least two orders of magnitude higher than the Kolmogorov time scale $\tau_K = (\nu/\bar{\varepsilon})^{1/2} \approx 0.05$ s. Following Eq. (2) in Kolmogorov (1962) the variance σ_ε^2 of the natural logarithm of ε_τ increases with decreasing τ. That means local values of ε_τ with $\tau \approx \tau_k$ might be significant higher than estimated from our measurements.

The observation of high Taylor Reynolds number resulting in high intermittency of ε_τ shows also the general limitation for direct numerical simulations (DNS) for investigations of turbulence–particle interactions. The largest DNS of turbulent flows reached ${\rm Re}_\lambda \sim 10^3$ (Kaneda et al. 2003) whereas DNS studies of particle-laden turbulence are limited to ${\rm Re}_\lambda \sim 10^2$ (e.g., Ferrante and Elgobashi 2003; Squires and Eaton 1991) which is about two orders of magnitude smaller than observed in our data. Therefore, results concerning particle–turbulence interaction obtained from DNS have to be interpreted with caution.

6. Summary

From earlier airborne studies of turbulence in clouds only data with a resolution of several meters are available. Therefore, only mean energy dissipation rates averaged over a complete flight lag were reported. In this work, turbulence data with a resolution on decimeter scales are presented for two measurement campaigns (BBC2 and INSPECTRO2). The two datasets represents two types of small cumulus fields at different

stages of development. The aim of this work was to test the hypotheses whether turbulence in clouds can be described with the same methods as used for intermittent (but cloud-free) flows.

Power spectra show an inertial subrange behavior down to length scales of about 0.2 m. For length scales between 0.8 and 80 m the ratios of $S(f)$ of longitudinal and transversal wind velocity components are close to the theoretical value of 4/3 indicating local isotropy. Deviations for smaller scales are due to general limitations of the measurements.

For the BBC2 data, high values of ε_τ were found in clouds in association with high turbulent activity due to vertical updrafts. For the observations during INSPECTRO2, highest ε_τ values were found in cloud gaps and mostly small values were observed in homogeneous parts inside the clouds. For this case, the vertical wind speed showed no significant correlation with the LWC indicating an "old" advected cloud. The higher ε_τ values between the clouds or in regions with cloud holes may be a signature of lateral mixing at cloud edges.

These differences between the two datasets become most evident in PDFs derived from data conditionally sampled on the LWC. For the BBC2 data, the average of ε_τ measured in clouds is about 5 times higher than for cloud-free regions, whereas there is no significant difference for the INSPECTRO2 data. However, $\bar{\varepsilon}_\tau$ averaged over the entire record was similar for both records.

Probability density functions of wind velocity increments are derived. The PDFs show significant deviations from a Gaussian distribution consistent with strong intermittency. The shape of the ε_τ PDFs could be parameterized with a lognormal distribution that is in good agreement with theory (Kolmogorov 1962) and earlier experiments made in the cloud-free boundary layer (Shaw and Oncley 2001). From these data we conclude that small-scale turbulence in clouds at least to decimeter scales can be well described with the same methods as used for cloud-free conditions.

Acknowledgments. We thank G. Sanftleben and his crew from the German Bundeswehr Technical Centre for Ships and Naval Weapons for the balloon operation. D. Schell from the enviscope GmbH (Frankfurt/Main) is acknowledged for his technical support during both experiments. Thanks are also due to R. Shaw, O. Hellmuth, and the two anonymous reviewers for their helpful comments on an earlier version of the manuscript. Finally, we thank KNMI, Netherlands, for hosting the BBC2 campaign and providing the radiosonde data.

REFERENCES

Ackerman, B., 1967: The nature of the meteorological fluctuations in clouds. *J. Appl. Meteor.,* **6,** 61–71.

Batchelor, G. K., 1953: *The Theory of Homogenous Turbulence.* Cambridge University Press, 197 pp.

Biltoft, C. A., 2001: Some thoughts on local isotropy and the 4/3 lateral to longitudinal velocity spectrum ratio. *Bound.-Layer Meteor.,* **100,** 393–404.

Blanc, T. V., W. J. Plant, and W. C. Keller, 1989: The Naval Research Laboratory's air–sea interaction blimp experiment. *Bull. Amer. Meteor. Soc.,* **70,** 354–364.

Böttcher, F., C. Renner, H.-P. Waldl, and J. Peinke, 2003: On the statistics of wind gusts. *Bound.-Layer Meteor.,* **108,** 163–173.

Brenguier, J.-L., 1993: Observations of cloud microstructure at the centimeter scale. *J. Appl. Meteor.,* **32,** 783–793.

——, T. Bourrianne, A. A. Coelho, J. Isbert, R. Peytavi, D. Trevarin, and P. Weschler, 1998: Improvements of droplet size distribution measurements with the fast-FSSP (forward scattering spectrometer probe). *J. Atmos. Oceanic Technol.,* **15,** 1077–1090.

Champagne, F. H., C. A. Friehe, J. C. LaRue, and J. Wyngaard, 1977: Flux measurements, flux estimation techniques, and fine-scale turbulence measurements in the unstable surface layer over land. *J. Atmos. Sci.,* **34,** 515–530.

Crewell, S., and Coauthors, 2004: The BALTEX Bridge Campaign: An integrated approach for a better understanding of clouds. *Bull. Amer. Meteor. Soc.,* **85,** 1565–1584.

Edson, J. B., A. A. Hinton, K. E. Prada, J. E. Hare, and C. W. Fairall, 1998: Direct covariance flux estimates from mobile platforms at sea. *J. Atmos. Oceanic Technol.,* **15,** 547–562.

Elgobashi, S., and C. Truesdell, 1993: On the two-way interaction between homogeneous turbulence and dispersed solid particles. I: Turbulence modification. *Phys. Fluids,* **5,** 1790–1801.

Ferrante, A., and S. Elgobashi, 2003: On the physical mechanisms of two-way coupling in particle laden isotropic turbulence. *Phys. Fluids,* **15,** 315–329.

Frehlich, R., Y. Meillier, M. L. Jensen, and B. Balsley, 2004: A statistical description of small-scale turbulence in the low-level nocturnal jet. *J. Atmos. Sci.,* **61,** 1079–1085.

Frisch, U., 1995: *Turbulence—The Legacy of A. N. Kolmogorov.* Cambridge University Press, 296 pp.

Gerber, H., 1986: Tethered balloon measurements at San Nicolas Island (Oct. 1984): Instrumentation, data summary, preliminary data interpretation. NRL Tech. Rep. 8972, Naval Research Laboratory, Atmospheric Physics Branch, Space Science Division, 29 pp.

——, 1991: Direct measurement of suspended particulate volume concentration and far-infrared extinction coefficient with a laser-diffraction instrument. *Appl. Opt.,* **30,** 4824–4831.

——, B. G. Arends, and A. S. Ackerman, 1994: New microphysics sensor for aircraft use. *Atmos. Res.,* **31,** 235–252.

——, J. B. Jensen, A. B. Davis, A. Mashak, and W. J. Wiscombe, 2001: Spectral density of cloud liquid water content at high frequencies. *J. Atmos. Sci.,* **58,** 497–503.

Haman, K., S. P. Malinowski, A. Makulski, B. D. Struś, R. Busen, A. Stefko, and H. Siebert, 2000: A family of ultrafast aircraft thermometers for warm and supercooled clouds and various types of aircraft. Preprints, *13th Int. Conf. on Clouds and Precipitation,* Reno, NV, International Commission on Clouds and Precipitation, 224–227.

——, ——, B. D. Struś, R. Busen, and A. Stefko, 2001: Two new

types of ultrafast aircraft thermometer. *J. Atmos. Oceanic Technol.,* **18,** 117–134.

Hill, R. J., 2002: Scaling of acceleration in locally isotropic turbulence. *J. Fluid Mech.,* **452,** 361–370.

Kaimal, J. C., and J. J. Finnigan, 1994: *Atmospheric Boundary Layer Flows.* Oxford University Press, 289 pp.

——, J. C. Wyngaard, and D. A. Haugen, 1968: Deriving power spectra from a three-component sonic anemometer. *J. Appl. Meteor.,* **7,** 827–837.

——, ——, Y. Izumi, and O. R. Cote, 1972: Spectral characteristics of surface-layer turbulence. *Quart. J. Roy. Meteor. Soc.,* **98,** 563–589.

Kaneda, Y., T. Ishihara, M. Yokokawa, K. Itakura, and A. Uno, 2003: Energy dissipation rate and energy spectrum in high resolution direct numerical simulations of turbulence in a periodic box. *Phys. Fluids,* **15,** L21–L24, doi:10.1063/1.1539855.

Kitchen, M., and S. J. Caughey, 1981: Tethered-balloon observations of the structure of small cumulus clouds. *Quart. J. Roy. Meteor. Soc.,* **107,** 853–874.

Kolmogorov, A. N., 1941: The local structure of turbulence in incompressible viscous fluid for very large Reynolds numbers. *Dokl. Akad. Nauk SSSR,* **30,** 301–304.

——, 1962: A refinement of previous hypotheses concerning the local structure of turbulence in a viscous incompressible fluid at high Reynolds number. *J. Fluid Mech.,* **13,** 82–85.

Lenschow, D. H., 1986: Aircraft measurements in the boundary layer. *Probing the Atmospheric Boundary Layer,* D. H. Lenschow, Ed., Amer. Meteor. Soc., 239 pp.

——, M. Zhou, X. Zeng, L. Chen, and X. Xu, 2000: Measurements of fine-scale structures at the top of marine stratocumulus. *Bound.-Layer Meteor.,* **97,** 331–357.

MacPherson, J. I., and G. A. Isaac, 1977: Turbulent characteristics of some Canadian cumulus clouds. *J. Appl. Meteor.,* **16,** 81–90.

Muschinski, A., R. G. Frehlich, M. L. Jensen, R. Hugo, A. M. Hoff, F. Eaton, and B. B. Balsley, 2001: Fine-scale measurements of turbulence in the lower troposphere: An intercomparison between a kite- and balloon-borne and a helicopter-borne measurement system. *Bound.-Layer Meteor.,* **98,** 219–250.

——, ——, and B. B. Balsley, 2004: Small-scale and large-scale intermittency in the nocturnal boundary layer and the residual layer. *J. Fluid Mech.,* **515,** 319–351.

Nicholls, S., 1984: The dynamics of stratocumulus: Aircraft observations and comparisons with a mixed layer model. *Quart. J. Roy. Meteor. Soc.,* **110,** 783–820.

——, and J. Leighton, 1986: An observational study of the structure of stratiform cloud sheets: Part I. Structure. *Quart. J. Roy. Meteor. Soc.,* **112,** 431–460.

Oboukhov, A. M., 1962: Some specific features of atmospheric turbulence. *J. Fluid Mech.,* **13,** 77–81.

Oncley, S., C. A. Friehe, J. C. Larue, J. A. Businger, E. C. Itsweire, and S. S. Chang, 1996: Surface-layer fluxes, profiles, and turbulence measurements over uniform terrain under near-neutral conditions. *J. Atmos. Sci.,* **53,** 1029–1043.

Pinsky, M. B., and A. P. Khain, 2004: Collision of small drops in a turbulent flow. Part II: Effects of flow accelerations. *J. Atmos. Sci.,* **61,** 1926–1939.

Plant, W. J., W. C. Keller, V. Hesany, K. Hayes, K. W. Hoppel, and T. V. Blanc, 1998: Measurements of the marine boundary layer from an airship. *J. Atmos. Oceanic Technol.,* **15,** 1433–1458.

Pope, S. B., 2000: *Turbulent Flows.* Cambridge University Press, 771 pp.

Saddoughi, S. G., and S. V. Veeravalli, 1994: Local isotropy in turbulent boundary layers at high Reynolds numbers. *J. Fluid Mech.,* **268,** 333–372.

Schmidt, S., K. Lehmann, and M. Wendisch, 2004: Minimizing instrumental broadening of the drop size distribution with the M-Fast-FSSP. *J. Atmos. Oceanic Technol.,* **21,** 1855–1867.

Shaw, R. A., 2000: Supersaturation intermittency in turbulent clouds. *J. Atmos. Sci.,* **57,** 3452–3456.

——, 2003: Particle-turbulence interactions in atmospheric clouds. *Annu. Rev. Fluid Mech.,* **35,** 183–227.

——, and S. P. Oncley, 2001: Acceleration intermittency and enhanced collision kernels in turbulent clouds. *Atmos. Res.,* **59–60,** 77–87.

——, W. C. Reade, L. R. Collins, and J. Verlinde, 1998: Preferential concentration of cloud droplets by turbulence: Effects on the early evolution of cumulus cloud droplet spectra. *J. Atmos. Sci.,* **55,** 1965–1976.

Siebert, H., and U. Teichmann, 2000: The behaviour of an ultrasonic under cloudy conditions. *Bound.-Layer Meteor.,* **94,** 165–169.

——, and A. Muschinski, 2001: Relevance of a tuning-fork effect for temperature measurements with the Gill Solent HS ultrasonic anemometer-thermometer. *J. Atmos. Oceanic Technol.,* **18,** 1367–1376.

——, M. Wendisch, T. Conrath, U. Teichmann, and J. Heintzenberg, 2003: A new tethered balloon-borne payload for fine-scale observations in the cloudy boundary layer. *Bound.-Layer Meteor.,* **106,** 461–482.

Smith, S. A., and P. P. Jonas, 1995: Observations of the turbulent fluxes in fields of cumulus clouds. *Quart. J. Roy. Meteor. Soc.,* **121,** 1185–1208.

Squires, K. D., and J. K. Eaton, 1991: Preferential concentration of particles by turbulence. *Phys. Fluids,* **3,** 1169–1178.

Sreenivasan, K. R., and R. A. Antonia, 1997: The phenomenology of small-scale turbulence. *Annu. Rev. Fluid Mech.,* **29,** 435–472.

Telford, J. W., and J. Warner, 1962: On the measurement from aircraft of buoyancy and vertical air velocity in cloud. *J. Atmos. Sci.,* **19,** 415–423.

Vaillancourt, P. A., and M. K. Yau, 2000: Review of particle–turbulence interactions and consequences for cloud physics. *Bull. Amer. Meteor. Soc.,* **81,** 285–298.

Vohl, O., S. K. Mitra, S. Wurzler, and H. R. Pruppacher, 1999: A wind tunnel study of the effect of turbulence on the growth of cloud drops by collision and coalescence. *J. Atmos. Sci.,* **56,** 4088–4099.

Willis, G. E., and J. W. Deardorff, 1976: On the use of Taylor's translation hypothesis for diffusion in the mixed layer. *Quart. J. Roy. Meteor. Soc.,* **102,** 817–822.

Wills, J. A. B., and L. R. Cole, 1986: Model studies of wind flow distortion on an AI600 airship. Tech. Rep. 45046, British Maritime Technology, Middlesex, United Kingdom, 15 pp.